JGR Oceans

RESEARCH ARTICLE
10.1029/2024JC020951

Deep Kinetic Energy Response to the Variability of the Kuroshio Extension

Jie-Hong Han[1,2,3], Yongsheng Xu[1,4,5,6], Chao Huang[1,5], Jianping Li[3,4], and Kai-Yuan Li[7]

[1]Key Laboratory of Ocean Observation and Forecasting, Key Laboratory of Ocean Circulation and Waves, Institute of Oceanology, Chinese Academy of Sciences, Qingdao, China, [2]Department of Ocean Science and Center for Ocean Research in Hong Kong and Macau, The Hong Kong University of Science and Technology, Hong Kong, China, [3]Frontiers Science Center for Deep Ocean Multispheres and Earth System and Key Laboratory of Physical Oceanography and Academy of the Future Ocean, Ocean University of China, Qingdao, China, [4]Laoshan Laboratory, Qingdao, China, [5]Center for Ocean Mega-Science, Chinese Academy of Sciences, Qingdao, China, [6]College of Marine Sciences, University of Chinese Academy of Sciences, Beijing, China, [7]Department of Earth and Planetary Sciences, University of California, Riverside, CA, USA

Abstract The transfer of energy from the upper to deep oceans is a well-known and challenging subject in physical oceanography. This research investigates the intricate relationship between surface and deep ocean currents. Utilizing nearly 2 years of observations from the Kuroshio Extension System Study (KESS), our study unveils the deep-ocean kinetic energy response to the Kuroshio Extension (KE) variability. We introduce the Kuroshio Extension Jet Path Index (KEJPI), which identifies two distinct modes of the KE jet on an intra-seasonal timescale. Our findings reveal a strong correlation (0.73) between KEJPI and the mean kinetic energy of deep-ocean geostrophic circulation, suggesting that the KE jet's large amplitude meanders have a significant impact on deep-ocean kinetic energy. Singular Value Decomposition (SVD) analysis further unveils a co-evolving spatial pattern between upper and lower ocean kinetic energy. We investigate the dynamic vertical coupling (DVC) mechanism by examining the coherent variation among the sea surface height (SSH), 15°C isotherm (Z15), deep pressure anomaly, and abyssal flow. The KE jet migration can induce net divergence and convergence within the water column, which in turn generates deep-ocean quasi-geostrophic currents. These currents show a marked increase in kinetic energy, reaching levels three times higher than the background. This DVC-driven kinetic energy can further cascade into near-inertial and high-frequency internal waves, contributing to abyssal mixing. Our study underscores the role of large current system instabilities in transferring energy to the deep ocean and facilitating deep mixing processes.

Plain Language Summary The transport of energy from the upper to deep oceans is a well-known and difficult topic in physical oceanography. However, the limit of observation on the deep-ocean circulations makes it the most uncertain process in the complex climate system. From 2004 to 2006, the Kuroshio Extension System Study used the in-situ measurement to investigate the characteristics and dynamics of the deep circulation at 5,300–6,400 m depth. The Kuroshio Extension (KE) jet exhibits two distinct modes, ranging from stable to unstable and back to stable during observations. The state of the KE jet has a strong impact on the variations and distributions of upper- and deep-ocean kinetic energy, indicating the coupled variation between the upper- and deep-ocean circulations. The deep-ocean kinetic energy increased to three times its original value when the KE jet became unstable. The co-volved process of sea surface height, vertical movement within the thermocline, deep-ocean pressure anomalies and deep-ocean kinetic energy is introduced to get insight into the underlying mechanism. Our research emphasizes the substantial influence of upper-ocean mesoscale processes on deep-ocean energy regulation. Furthermore, we identify potential hot spots for deep-ocean energy transfer and diapycnal mixing contributions, particularly in regions with robust ocean currents.

Key Points:

- Deep ocean kinetic energy shows significant response to KE jet variability
- Energy cascade can be promoted in the deep-sea kinetic energy response
- Dynamic vertical coupling mechanism is proposed to understand the response

Supporting Information:

Supporting Information may be found in the online version of this article.

Correspondence to:

Y. Xu,
yongsheng.xu@alumni.caltech.edu

Citation:

Han, J.-H., Xu, Y., Huang, C., Li, J., & Li, K.-Y. (2024). Deep kinetic energy response to the variability of the Kuroshio Extension. *Journal of Geophysical Research: Oceans*, *129*, e2024JC020951. https://doi.org/10.1029/2024JC020951

Received 21 JAN 2024
Accepted 16 SEP 2024

Author Contributions:

Conceptualization: Jie-Hong Han, Yongsheng Xu
Formal analysis: Jie-Hong Han
Funding acquisition: Yongsheng Xu
Investigation: Jie-Hong Han
Methodology: Jie-Hong Han, Yongsheng Xu, Jianping Li
Supervision: Yongsheng Xu
Validation: Jie-Hong Han
Visualization: Jie-Hong Han, Kai-Yuan Li
Writing – original draft: Jie-Hong Han, Yongsheng Xu
Writing – review & editing: Jie-Hong Han, Yongsheng Xu, Chao Huang, Jianping Li, Kai-Yuan Li

1. Introduction

An important advance in modern physical oceanography is the recognition that the main driving force for the return of deep ocean water to the surface is the mechanical energy available for deep ocean mixing (Munk & Wunsch, 1998; Polzin et al., 1997; Waterhouse et al., 2014). The buoyancy gain from abyssal mixing needs to balance the sinking-induced bottom water formation. Munk and Wunsch (1998) argued that wind energy input to oceanic circulation can be transferred down to the deep ocean, accounting for 50% of the mechanical energy available for deep ocean mixing. Several studies have quantified the wind power input (WPI) to the upper ocean

circulation with diverse data and methodologies (Munk & Wunsch, 1998; Scott & Xu, 2009). Although the regional distribution of the WPI changes after accounting for ocean current effects on wind stress, the WPI for the global ocean is estimated to be around 1 TW (Munk & Wunsch, 1998; Xu & Scott, 2008). The WPI raises the potential energy of the large-scale flow, which subsequently cascades its energy into mesoscale variability. However, the specific processes and mechanisms by which this mesoscale variation in upper ocean energy affects the deep-sea circulation are still in need of further investigation. This topic, crucial to understanding the cycling of deep-sea fluids back to the surface, carries substantial implications for our comprehension of climate dynamics.

Increasing evidence from observational and modeling studies indicates that mesoscale variabilities in the upper ocean affect deep ocean flows (Adams & Flierl, 2010; Liang & Thurnherr, 2011; Petersen et al., 2013; Xu et al., 2009; Zhang et al., 2013, 2015). Utilizing a single-point mooring observation on the seafloor, several studies applied dynamical mode analysis to examine the velocity change at various depths as surface-generated eddies passed (Hu et al., 2020; Liang & Thurnherr, 2011; Zhang et al., 2013). However, mode analysis, similar to Fourier transform analysis, can only be used to analyze patterns and regularities in data, not to explain the mechanisms behind the occurrence of the signal. The underlying physical mechanism remains unknown. Numerical studies suggest that pressure work may play an important role in linking upper- and deep-ocean mesoscale variability (e.g., Cai & Gan, 2021; Yang et al., 2021). With mesoscale resolution, the CPIES (current and pressure recording inverted echo sounders) array, consisting of current meters, bottom pressure gauges, and inverted echo sounders, is capable of observing synchronized dynamic phenomena in both the upper and deep ocean over extensive areas. Shay et al. (1995) and Watts et al. (1995) used CPIES to demonstrate that Gulf Stream meander troughs (crests) developed and intensified jointly with deep cyclones (anticyclones). Savidge and Bane (1999) analyzed the vertical coupling process by examining the conservation of potential vorticity and the net convergence/divergence in the geostrophic fluid. They draw a comparison between this process and atmospheric cyclogenesis. Their research highlights that changes in upper-ocean circulations contribute to the development of deep-ocean cyclones through the net divergence of the entire water column. From 2004 to 2006, a multi-institutional collaborative project, the Kuroshio Extension System Study (KESS) used the CPIES to investigate the characteristics and dynamics of the deep circulation at 5,300–6,400 m depth (e.g., Bishop, 2013; Greene et al., 2012; Na et al., 2016; Tracey et al., 2012). Unlike studies in the Gulf Stream, the rough and intricate topography of the Kuroshio Extension (KE) region leads to the elusiveness of studies related to the processes of covariation of the upper- and deep-ocean circulations in this region. Greene et al. (2012) attempted to combine the effect of topography to investigate the coupled process between upper- and deep-ocean variability. However, none of these studies have elaborated on the connection between the upper- and deep-ocean energy. How deep-sea kinetic energy responds to the variability of upper-ocean KE jet remains an open question.

In this study, using the observations from the 2 year CPIES array from KESS, we focus on the deep kinetic energy response to the variability of the Kuroshio Extension. We first illustrate the KE jet variability on an intra-seasonal scale, which has two distinct modes. The variability of the upper-ocean jet governs the distribution pattern of kinetic energy in the upper-ocean. We present three case studies to illustrate how upper-ocean KE jet great meanders produced vertical motions within thermocline, resulting in variations in deep-ocean currents. The enhanced deep-ocean energy further cascades into the small-scale motion, which contributes to the deep-ocean diapycnal mixing. This paper aims to illustrate the response of deep kinetic energy to the variability of the KE and to identify the mechanisms that drive this connection.

2. Data and Methodology

The SSH data is from the Copernicus Marine Environment Monitoring Service (CMEMS). The climatological KE jet path is obtained by this satellite observed SSH data (1993–2012). From May 2004 to July 2006, KESS was conducted to identify and quantify the dynamic processes governing the variability of the KE and the recirculation gyre. Forty-six current and pressure recording inverted echo sounders were moored in the depth under 5,000 m in the KE region, 32–37°N, 143–149°E (Figure 1). CPIES equipped with Aanderaa Doppler current sensor tethered 50 m above the bottom, pressure sensor and inverted echo sounder aims to measure the deep ocean velocity (u, v), deep pressure variations (p) and the vertical acoustic travel time (τ) round trip from the seafloor to the surface and back. Variations in τ arise are mainly caused by the changes in thermocline depth. All the measured variables τ, p, u and v, were processed to an hourly output interval. The latest CPIES processing techniques, assessment of the KESS array's performance and data quality are discussed in Donohue et al. (2010) and Kennelly et al. (2008)

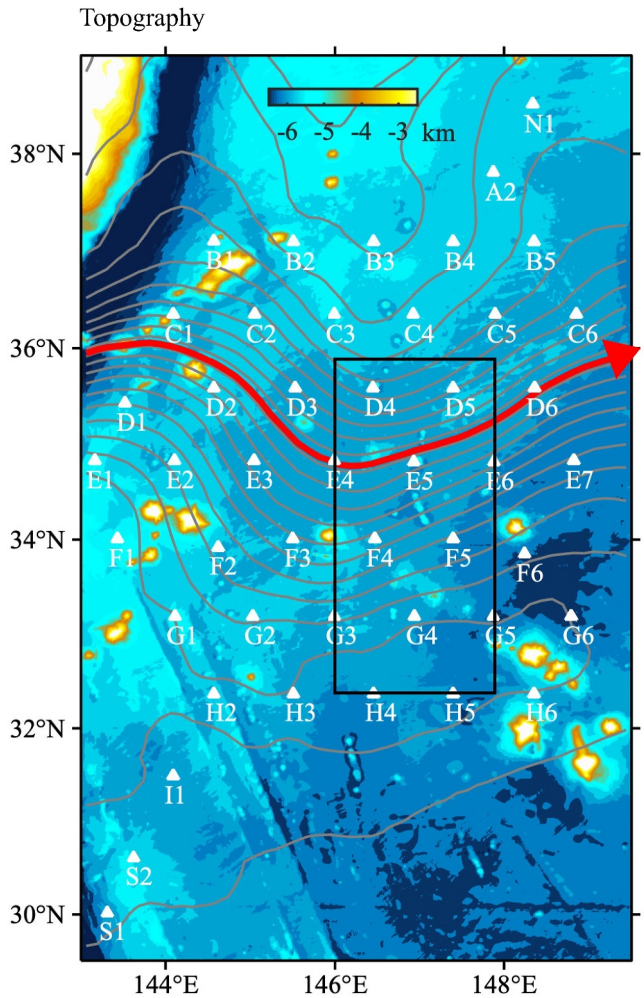

Figure 1. 2-D seabed topography near the KESS, with the KESS observational array (white triangle), key region (black box), the climatological SSH pattern (gray contour), and the KE jet path (red line, obtained from CMEMS satellite-observed SSH).

comprehensively. We use data between May 2004 to October 2005 for analysis in this study, for most of the observatories were in operation only until the end of 2005.

Following techniques described by Watts et al. (2001) and Donohue et al. (2010), the bottom pressure and velocity were jointly mapped using multivariate optimal interpolation. The pressure field (P) can be converted to deep streamfunction:

$$\psi_D = P/\rho f$$

where ρ and f are respectively the average deep density and the Coriolis parameter. Previous research has demonstrated that τ could be used to estimate geopotential height (ϕ) (Andres et al., 2008; Meinen & Watts, 2000; Watts & Johns, 1982; Watts & Rossby, 1977). 5,300 dbar was chosen as the level to the pressure gauges and ϕ (Donohue et al., 2010). Thus, τ is transferred into ϕ_{5300}, which was subsequently converted to upper-ocean streamfuction:

$$\psi_U = \phi_{5300}/f$$

After transferring ψ_U and ψ_D, the values are interpolated on a 1/8° grid. The ψ_U can also be transferred into sea surface height (SSH) in the KE region (Donohue et al., 2010).

The inverted echo sounder can be used to estimate vertical profiles of temperature and salinity using empirical relationships established with historical hydrography. The technical details are available in Donohue et al. (2010). Since the potential density variations are concentrated over a very short interval in the vertical, namely the permanent thermocline, such that the ocean is often considered to be a two-layer system (Savidge & Bane, 1999). The depth of the 15° isotherm (Z15) was used as an indicator of the boundary between the upper and the deep ocean. To better illustrate the mechanism of the study, we define w as downward as positive. The vertical movement of this boundary layer (w) signifies convergence or divergence in the upper ocean, accompanied by a contrasting effect—divergence or convergence—in the lower ocean.

In this study, we first investigate the coupled variability of relative low frequency (geostrophic scale) motion of the upper and deep ocean. The velocity of geostrophic circulations in upper ocean (u_1, v_1) and deep ocean (u_2, v_2) can be obtained from ψ_U and ψ_D, according to the geostrophic balance. The geostrophic circulation kinetic energy in the upper (*GEK_u*) and deep ocean (*GEK_d*) was defined as:

$$GEK\_u = \frac{1}{2}\left({u_1}^2 + {v_1}^2\right) \quad (1)$$

$$GEK\_d = \frac{1}{2}\left({u_2}^2 + {v_2}^2\right) \quad (2)$$

Singular value decomposition (SVD) analysis is used to describe the coupled variability of *GEK_u* and *GEK_d* in the KE region to find out the potential relationship between the upper-ocean KE jet variability and deep-ocean circulations. SVD analysis is thought of as a generalization to rectangular matrices of the diagonalization of a square symmetric matrix (i.e., EOF analysis). It is usually applied to two data fields together to identify pairs of coupled spatial patterns, which explains how much each pair of patterns contributes to the cross-covariance. The patterns are called singular vectors and they are spatially independent from each other. The first pair of singular vectors explains the largest part of the cross-covariance and the next pairs explain the remaining parts in

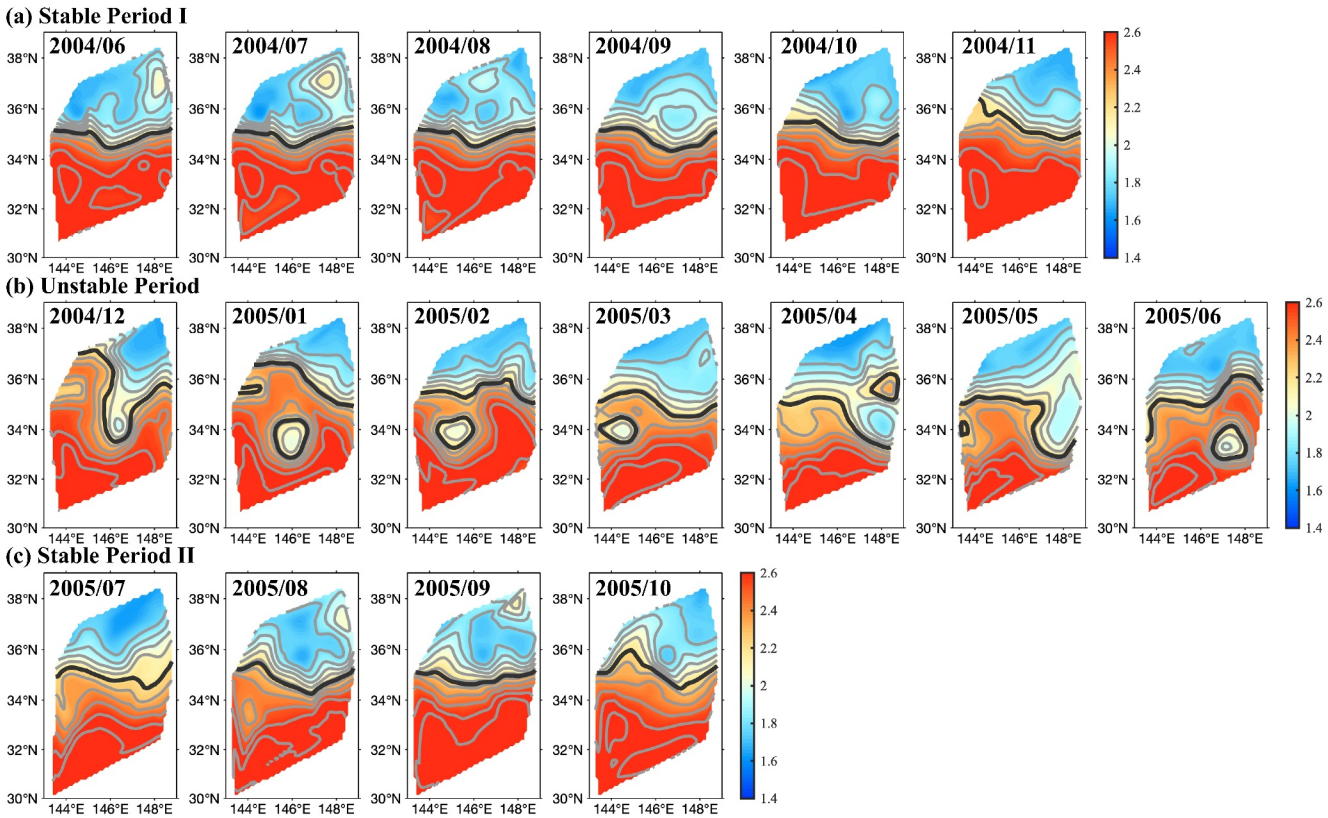

Figure 2. Maps of monthly average sea surface height field during the observation period. (a) Indicates the maps of the monthly average sea surface height field during June 2004–November 2004 when the path of Kuroshio Extension jet is stable. (b) as for (a), but for December 2004–June 2005 when the path of Kuroshio Extension jet is unstable. (c) as for (a), but for July 2005–Oct 2005 when the path of Kuroshio Extension jet is stable. Contour intervals are 0.1 m with thick lines denoting the 2.2 m contours (represents the paths of Kuroshio Extension jet).

decreasing order. The *k*th time series for each variable is obtained by projecting the *k*th singular vector onto the original data field. The correlation coefficient (*Corr.*) between the *k*th time series of the two variables indicates how strongly related the coupled patterns are. This technique is widely used in geophysics research (Kohyama et al. (2021); Venegas et al., 1997; Wallace et al., 1992).

According to different frequency bands, the deep-ocean flows were divided into three types: flows with low frequencies (LF, period >3 days), flows with NIW frequencies [(0.85, 1.2) f, f is local inertial frequency], and flows high frequencies (HF, >1.2 f). The kinetic energy (EK) of each observation site is estimated by the equation:

$$EK = \frac{1}{2}\rho\left(u^2 + v^2\right) \tag{3}$$

where ρ is the density of the seawater, u and v are the zonal and meridional velocity observed by Aanderaa Doppler current sensors from the observation sites.

3. Deep Kinetic Energy Response to KE Variability

3.1. Upper KE Variability and Deep Kinetic Energy Response

To explore the changes in the KE jet and its surrounding areas, we begin with Figure 2 showing the monthly averaged SSH fields between June 2004 to October 2005. As illustrated by the black lines in Figure 2, the paths of the KE jet are defined by the 2.2 m contours featured in the SSH maps. These contours consistently align with, or closely approximate, the maxima of the meridional gradient of SSH ($\partial SSH/\partial y$), thereby serving as a reliable indicator for determining the axis of the KE jet (Qiu & Chen, 2005). During June–November 2004, the spatial

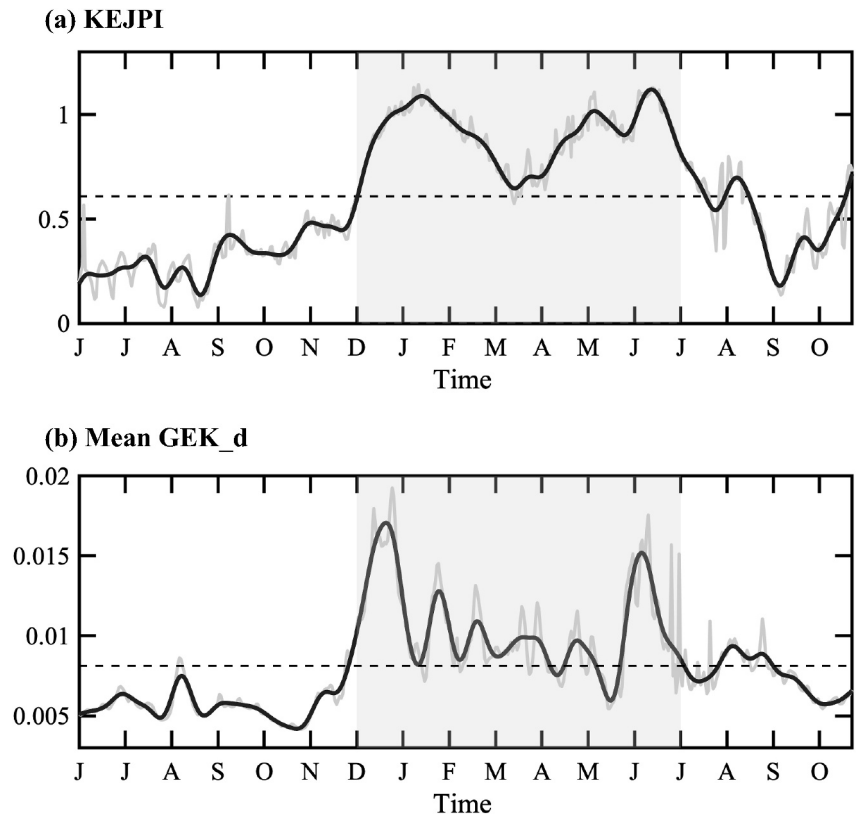

Figure 3. (a) The Kuroshio Extension Jet Path Index (KEJPI) during the observation period. The KEJPI is defined as the standard deviation of the latitude of the Kuroshio Extension jet path (2.2 m contours in SSH map) in the observation region. The black dashed line shows the mean value of the KEJPI during the observation period. (b) The *GEK_d* during the observation period. The black dashed line shows the mean value of *GEK_d* during the observation period. The black lines are the result of 21 day low-pass filtering from the original data (gray lines). The gray shaded period represents the unstable period from December 2004 to June 2005.

pattern of the monthly average SSH field closely resembles the climatological SSH pattern (Figure 1): the quasi-stationary meanders were well-developed between 34 and 36°N and the KE jet is relative stable (Figure 2a). This close-to-climatology SSH pattern, however, started to degenerate during December 2004 to June 2005. With large amplitude meanders, variable KE jet and the barely discernible southern recirculation, the SSH and KE jet pattern had almost no resemblance to that of the climatology (Figure 2b). From July–October 2005, the quasi-stationary meanders reemerged and the SSH patterns also became comparable to that of climatology. As indicated by previous research (Qiu & Chen, 2005), the KE jet exhibits two distinct modes, namely stable and unstable modes, on annual to decadal time scale. Nevertheless, our result from in-situ observation additionally provides the evidence that KE jet also exhibits distinct spatial patterns on an intra-seasonal time scale. Thus, we categorize the observation time into three distinct periods according to the variability of the KE jet (Stable Period I: June-November 2004; Unstable Period: December 2004 to June 2005; Stable Period II: July-October 2005).

To further quantify the variability of KE jet, especially its switching between different modes, we define the Kuroshio Extension Jet Path Index (KEJPI) from the standard deviation of the KE jet path (2.2 m contours from daily SSH data). Note that stable and quasi-stationary meanders of KE jet path are relatively straight in zonal direction, indicating that its variability is reduced compared to the larger amplitude meanders observed during the Unstable Period. Therefore, a higher value in Figure 3a indicates a more convoluted path taken by the KE jet. It is very clear from the time series of KEJPI that the KE jet during the observation period exhibits two distinct modes: a stable mode characterized by a straight path, and an unstable mode characterized by a convoluted with seasonal variations (gray shaded period in Figure 3a) resulting from the shedding and merging of mesoscale eddies. As Figure 3a shows, the stable mode of KE jet existed before December 2004 and after July 2005, whereas the

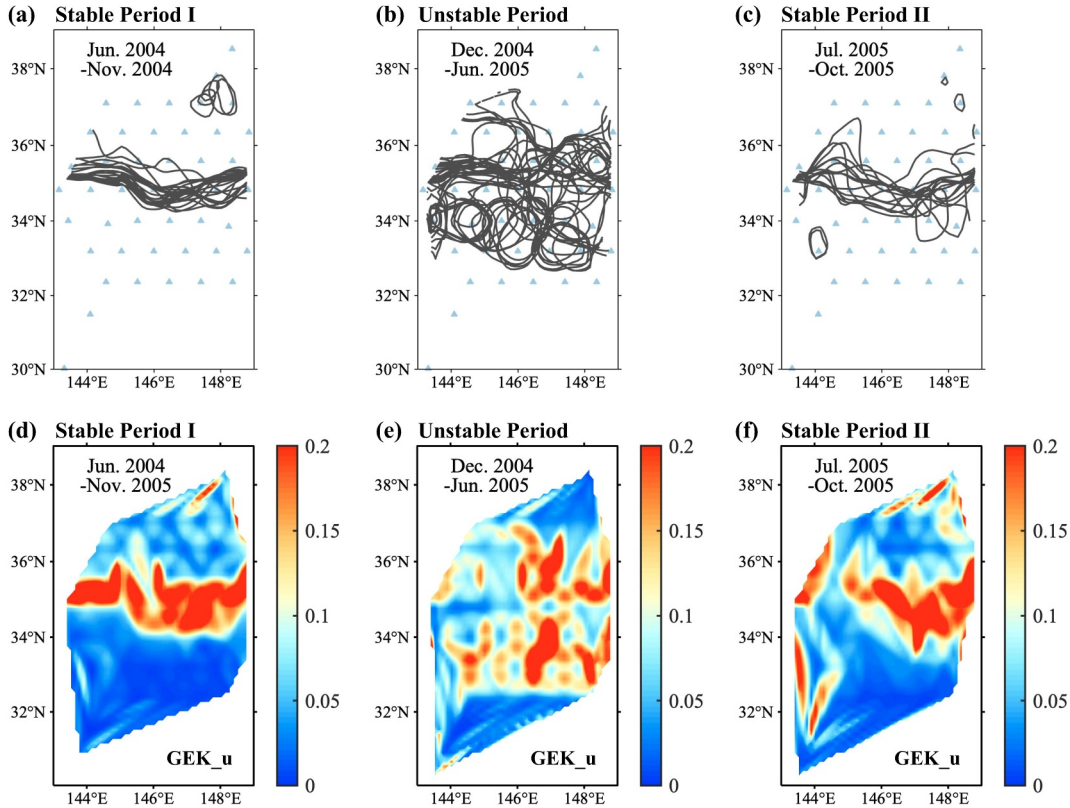

Figure 4. The paths of the Kuroshio Extension jet and the corresponding geostrophic circulations kinetic energy in the upper ocean (*GEK_u*) during different periods. (a) The jet paths between June 2004 - November 2004 are defined by the 2.2 m contours in the weekly SSH fields, plotted every 7 days (b), (c) as for (a), but for December 2004–June 2005 and July 2005–October 2005, respectively. Blue triangles denote the observational array. (d) The geostrophic kinetic energy in the upper ocean (*GEK_u*) during June 2004–November 2004. (e), (f) as for (d), but for December 2004–June 2005 and July 2005–October 2005, respectively (unit: m^2/s^2).

unstable mode existed from December 2004 to June 2005. This result aligns with our established criteria for identifying stable and unstable periods, as depicted in Figure 2.

By superimposing the snapshots of the KE jet paths in three different periods, we reveal the KE jet variability in its two distinct modes (Figure 4). During the Stable Period I and II, the KE jet path was mostly straight with minor deviations, primarily concentrated within the range of 34–36°N. Note that the paths of KE jet were more stable during Stable Period I than that in Stable Period II (Figures 4a and 4c). As expected, the KE jet path tends to be more variable during Unstable Period when the quasi-stationary meanders are obscure in the averaged SSH maps. The development of large amplitude meanders, along with the interaction with mesoscale processes, caused the path of KE jet to become chaotic. Correspondingly, the change of KE jet mode leads to the upper-ocean kinetic energy pattern regime shift (Figure 4). The upper-ocean geostrophic kinetic energy (*GEK_u*) concentrates along the main axis of KE jet (34–36°N) during the Stable Period I and II. However, when the KE jet switched to the unstable mode, the presence of baroclinic instability led to a significant meridional movement of the KE jet with a large amplitude. As a consequence, the upper-ocean geostrophic kinetic energy, which was previously concentrated in the climatological position of the KE jet, became dispersed and distributed on the northern and southern flanks of the jet (Figure 4b). This result shows that the upper-ocean KE jet variability has a strong impact on the upper-ocean energy distribution during the observation period, which was also observed in previous research (Qiu & Chen, 2005). Whether such upper-ocean energy regime shift can alter the flows in the deep ocean? As Figure 3b shows, the mean kinetic energy of deep-ocean geostrophic flows (*GEK_d*) also exhibits two distinct modes with alternating features. The *GEK_d* time series and the KEJPI co-evolve, with a correlation coefficient of 0.73 at the 95% confidence level, indicating the variable state of the upper-ocean KE jet may have a considerable implication on drastic alterations in deep-ocean flows and energy dynamics. Interestingly, KEJPI in Figure 3a doesn't exhibit

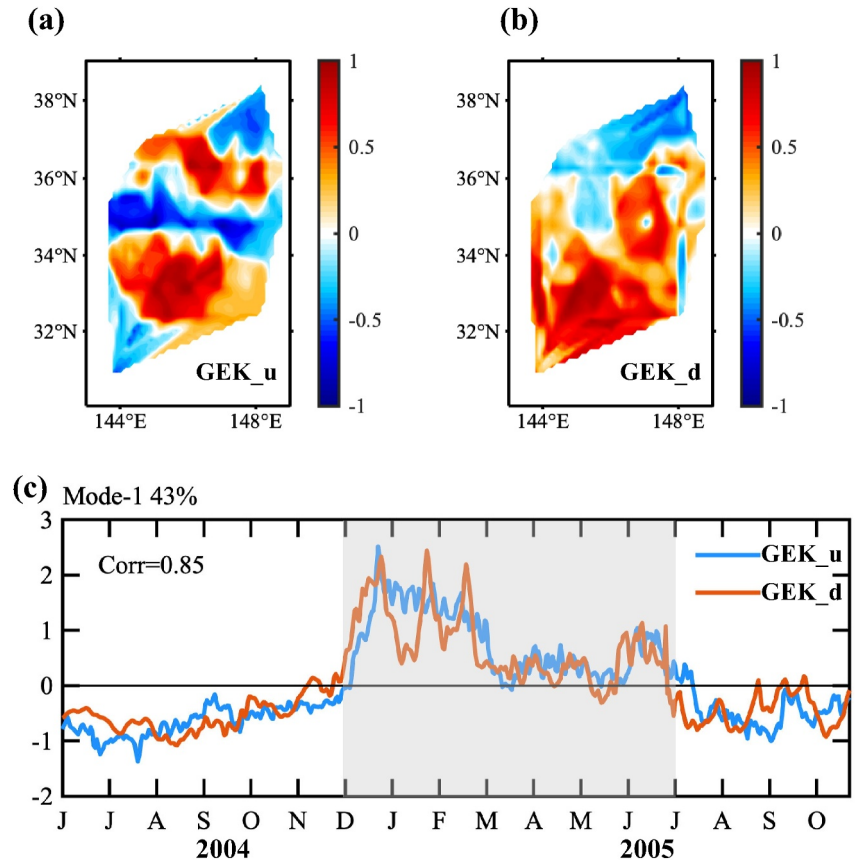

Figure 5. (a) and (b) Geostrophic circulations kinetic energy pattern extracted as the first mode of the SVD (SVD1) between the upper ocean (*GEK_u*) and deep ocean (*GEK_d*) in the observation region. (c) Projected geostrophic kinetic energy time series onto SVD1 for the *GEK_u* and *GEK_d*. Also shown is the correlation coefficient (Corr) between the two time series (0.85), which is above the 95% confidence level. The SVD1 explains 43% of the total variance present in the original data. The gray shaded period represents the unstable period from December 2004 to June 2005.

the same intra-seasonal variations as *GEK_d* in Figure 3b. This difference arises because the *GEK_d* is related to the variability of the KE path itself (Figure 4b), rather than simply the standard deviation of that variability (though the two are related). The identical KEJPI values (standard deviation of the KE jet path) may correspond to distinct KE jet patterns. The co-evolution of intra-seasonal variability within the KE jet path and deep energy will be revealed from the dynamic process in Section 3.3.

3.2. SVD Analysis of Upper- and Deep-Ocean Geostrophic Kinetic Energy

To understand the response of deep-ocean kinetic energy to the upper-ocean variability, we first conduct the SVD analysis on the upper- and deep-ocean geostrophic kinetic energy (*GEK_u* and *GEK_d*). The SVD, commonly referred to as maximum covariance analysis, extracts kinetic energy patterns that maximize the covariance between the two projected time series. Figure 5 shows the first mode of SVD (SVD1), which accounts for 43% of the total variance. It is the most important coupled mode of upper- and deep-ocean variability from the energy perspective. Figure 5a reveals a negative SVD1 anomaly between 34 and 36 ˚N, aligning with the KE jet's position in Figures 4a and 4c (stable periods). Figure 4b demonstrates that the KE path's back-and-forth migration primarily occurred south of 36 ˚N. Importantly, Figure 5b exhibits greater SVD1 *GEK_d* variability south of 36 ˚N, mirroring the KE jet's path fluctuations seen in Figure 4b. This implies that the deep-ocean circulation in this region is tightly coupled with the upper-ocean KE jet variability. It is a critical region for the upper-ocean energy to impact the deep-ocean flows in the Kuroshio Extension. Although their spatial patterns are different, the two time series extract from SVD1 display statistically significant correlations of 0.85 at the 95% confidence level, suggesting a concurrent and coupled fluctuation of the upper-ocean energy distribution pattern (regulated by KE

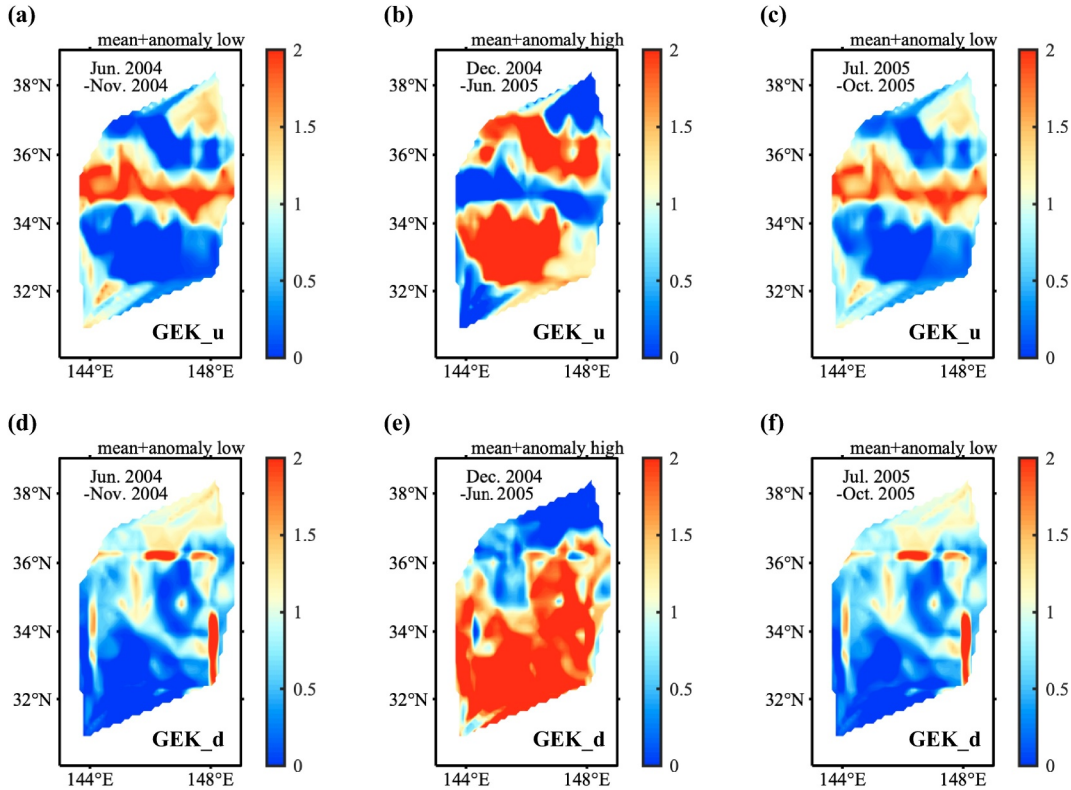

Figure 6. Coupled pattern pairs formed from SVD1 maps of *GEK_u* and *GEK_d* after restoring their respective time-mean field as detailed in text. (a), (b) and (c) denote the coupled pattern pairs of *GEK_u* during the three different periods. (d), (e) and (f) as for (a), (b) and (c), but for *GEK_d*. This figure represents the patterns of maximally correlated geostrophic circulation kinetic energy in the upper and deep ocean.

jet migration) and deep-ocean circulations energy. In addition, the two SVD1 time series exhibit a biphasic transition, whereby the value altered from negative to positive in November 2004 and then returned to negative in June 2005 (Figure 5c). They are identical to the KEJPI and time series of mean *GEK_d* seen in Figure 3. Hence, SVD analysis uncovers the interconnected and causal patterns of shifts in the upper-ocean KE jet regimes and alterations in deep-sea circulation.

How does the deep-ocean kinetic energy respond to the varying KE jet? Since the SVD mode is an anomaly mode relative to the time-averaged field, and the time index series represent the amplitudes and sign changes of the anomaly fields during the observation period (Xu et al., 2009). The time-averaged fields of SVD1s were added back to their time-varying anomaly fields in three different periods specified by KE jet variability to investigate the dynamic implications of the SVD1 *GEK_u* and *GEK_d* coupled pattern. We add *GEK_u* time mean fields to its SVD1 anomaly field multiplied by its negative extremum time-index values in Stable Period I and II separately, representing the stable mode of KE jet in that two period (Figures 6a and 6c). While *GEK_u* time mean fields were added to its SVD1 anomaly field multiplied by its positive extremum time-index values in Unstable Period which represent the upper-ocean kinetic energy responses to the unstable mode of KE jet (Figure 6b). The *GEK_u* patterns in different periods represent the alternating terminal patterns between which the *GEK_u* field fluctuates. Similarly, we obtain the corresponding three different SVD1 *GEK_d* patterns in the three periods (Figures 6d–6f). Figures 6a and 6c show the high value of SVD1 *GEK_u* concentrated in the climatological position of KE jet path during the stable period, which is nearly identical to Figures 4d and 4f. At the same periods, the SVD1 *GEK_d* is relatively low in the majority of the observed area (Figures 6d and 4f). During the Unstable Period, the SVD1 *GEK_u* near the climatological position of the KE jet decreased, whereas it increased significantly on its northern and southern sides (Figure 6b). This pattern is similar to the *GEK_u* pattern when the KE jet is unstable that large amplitude meanders develop and interact with mesoscale eddies (Figures 4b and 4e).

Correspondingly, the SVD1 *GEK_d* strengthened in the most observation area (south of 36˚N) (Figure 6e). It also suggests the deep-ocean currents energy source is upper-ocean KE jet instability.

The time series of mean *GEK_d* in Figure 3b closely resemble those of SVD1 and KEJPI, all of which exhibit two-stage variation. Furthermore, Figure S1 in Supporting Information S1 shows the difference in deep-ocean geostrophic circulations kinetic energy between the Unstable period and Stable period I, that is nearly identical to the SVD1 *GEK_d* pattern (Figure 5b). Thus, the SVD1 *GEK_d* reflects the variation of deep-ocean geostrophic circulations kinetic energy. This result shows compelling evidence that the fluctuations in upper-ocean KE jet have a substantial impact on the alterations in kinetic energy of deep-ocean geostrophic circulation. When the KE jet is stable with quasi-stationary meanders, the deep-ocean energy level is relatively low (~0.005 m^2/s^2) that deep-ocean flows are almost static. However, when the KE jet becomes unstable with a convoluted path and chaotic movement, the deep-ocean geostrophic kinetic energy strongly increased (maximum ~0.02 m^2/s^2), suggesting the transfer of energy from the upper-ocean to the deep-ocean currents.

3.3. Dynamic Vertical Coupling Mechanism

To investigate the process and mechanism of deep-ocean circulation kinetic energy response to the changing upper-ocean KE jet, we employ a time-latitude Hovmöller diagram (Figure 7). It depicts the vertical connection between the dynamics of the upper and deep oceans. Figure 7 shows coupled variation of the time-latitude section of SSH (reflects upper-ocean KE jet instability), vertical movement of Z15 (*w*, upward is negative, represents the boundary of the upper and lower layer in the ocean), deep pressure anomaly (reflects deep-ocean pressure response), and the kinetic energy time series from deep-ocean observatories. The SSH results also show that the KE jet undergoes three periods, transitioning from stable to unstable and back to stable state (Figure 7a), consistent with Figures 2 and 3a. Figure 7a shows the KE jet underwent three rapid meridional shifts during the Unstable Period. These three events were responsible for the highly unstable pattern of the KE jet during this period. We named the three events as Event1, Event2 and Evnet3. Other variables in the subsurface and deep ocean also exhibit the strongest signals and the notable changes during Unstable Period, particularly about these three events (Figures 7b and 7c). Deep-ocean current meters have detected a substantial increase in mean kinetic energy (MEK) in the deep ocean during the three events (Figures 7d and 7e). In Figure 7d, the E5 station exhibits the most significant kinetic response to the fluctuation of the upper-ocean KE jet. To eliminate the influence of this substantial number on the overall average, we exclude the E5 station from the calculation of MEK (Figure 7e). The result shows the enhancement of deep-ocean kinetic energy is also detected by the majority of the observation sites of the CPIES array in this area. It becomes evident that the MEK experiences a substantial rise in all three events (~3 times larger than that during Stable Period I and II), demonstrating that alterations in the KE jet can greatly enhance the total kinetic energy level in the deep ocean. The MEK during Stable Period is 4.05 J/m^3. However, it increased to 12.68, 13.52 and 15.01 J/m^3 in the three events (Figure 7e), respectively. The process of the co-evolution of upper-ocean KE jet, subsurface, deep-ocean physical fields, and kinetic energy can be referred to as the Dynamic Vertical Coupling (DVC) event. What is the main process of the DVC event? Alternatively, how can the DVC process effectively transfer energy to the deep ocean, given that a significant amount of the energy in the deep ocean originates from the upper ocean (Munk & Wunsch, 1998)?

The dashed outlines in Figures 7a–7c illustrate the connections between the KE jet SSH, the vertical movement at 15°C isotherm (Z15), and the deep pressure at 5,300 m. During the DVC events, the southward-moving KE jet, marked by white shading in Figure 7a, triggers a swift decrease in SSH, an ascent of Z15 at approximately 15 m per day (indicated by negative *w* values), and a low-pressure anomaly near the bottom of the trough region. In contrast, the northward-moving KE jet causes an increase in SSH, a descent of Z15 at around 20 m per day (indicated by positive *w* values), and a high-pressure anomaly near the bottom of the crest region. These observations suggest that pressure anomalies might be linked to the converging and diverging motions within the water column. Theoretically, a positive (negative) pressure anomaly should be associated with a net converging (diverging) motion within the water column.

Figures 8 and 9 further illustrate the DVC process in a two-dimensional view during the three events. In Event1, the KE jet showed an equatorward movement during the first 2 weeks, followed by a northward retraction in the following days (Figure 7a). Consequently, Event1 can be segmented into two phases: Event1_1 and Event1_2, depicted in Figures 8a and 8b, respectively. Figure 8a highlights the positional shifts of the KE jet at the beginning (dashed line) and end (solid black line) of Event1_1. During Event1_1, a distinct meandering trough formed

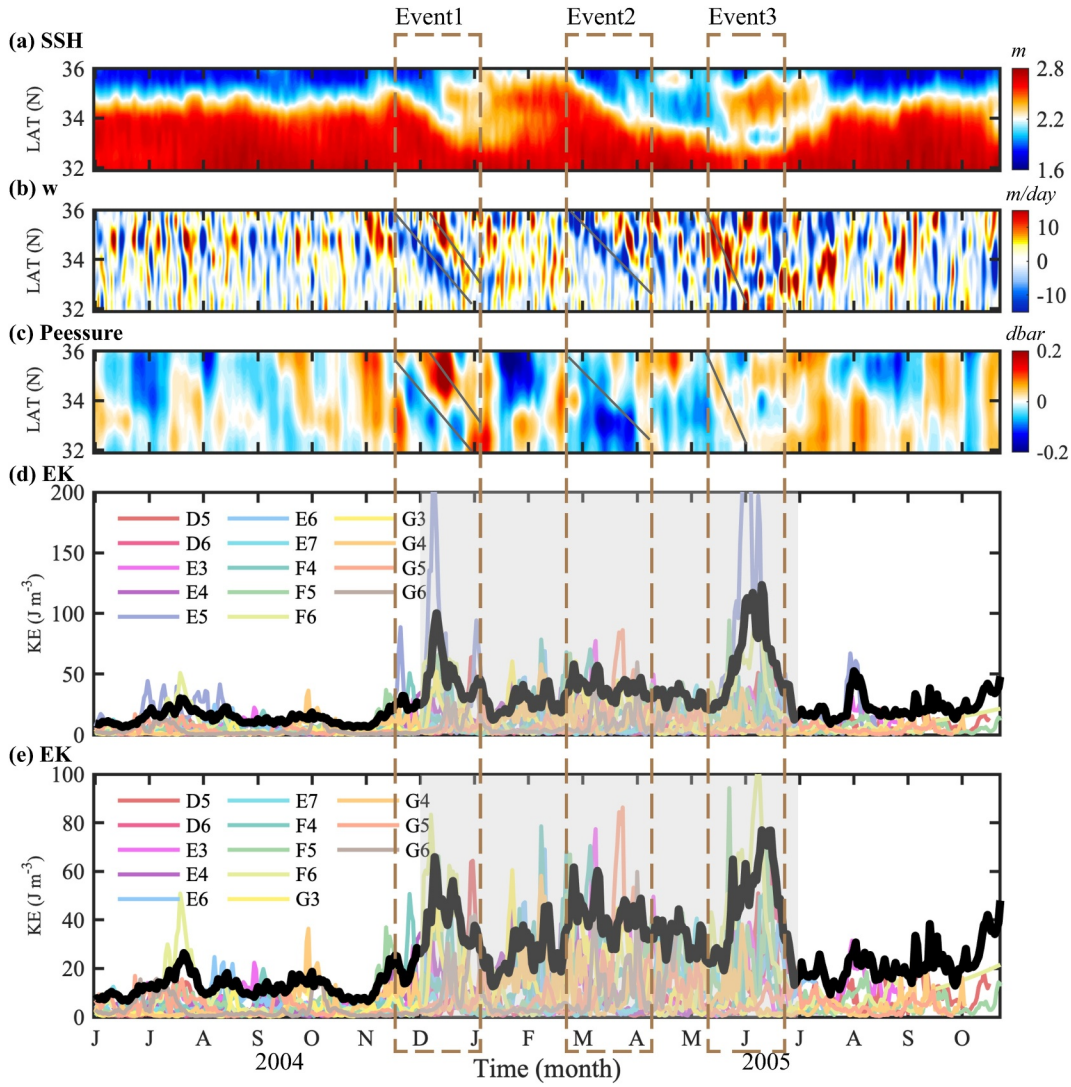

Figure 7. Coupled variation between the upper and deep ocean. (a) Hovmöller diagram (time-latitude contour) showing temporal variabilities of SSH from KESS observation key region (143–148°E, 32–36°N; the black box in Figure 1). White shading denotes the movement of Kuroshio Extension jet. (b), (c) as for (a), but for vertical velocity (w) of Z15 and deep-ocean pressure anomaly. The positive value in (b) indicates the downward movement of Z15, verse versa. (d) Time series of kinetic energy (EK) of the observation sites around the key region. The black line denotes the time series of three times mean kinetic energy (3 × MEK) of the observation sites around the key region. (e) As for (d), but the E5 station is excluded in the calculation. The gray shaded period represents the unstable period from December 2004 to June 2005. The three dashed boxes denote the three typical Vertical Coupling events during the observation period.

between 145.5 and 147.5°E, flanked by two distinct crests. During this phase, the southward moving trough led to a decrease in SSH over an area of 50–100 km, with a Z15 rise of 15 m per day and a negative pressure anomaly of −0.08 dbar. This pattern suggests divergence in the upper layer (from Z15 to the surface) and convergence in the lower layer. The crests, conversely, displayed an opposite pattern, marked by upper-layer convergence and lower-layer divergence (Figures S4a–b in Supporting Information S1). The presence of a negative (positive) pressure anomaly near the bottom of the trough (crest) region signifies a net divergence (convergence) within the entire water column. These pressure anomalies are capable of generating geostrophic currents in the deep ocean and contribute significantly to the increase in deep-ocean kinetic energy around their moving paths during Event1. This event underscores the critical role of the DVC process in the transfer of energy from the upper layer to the deep ocean.

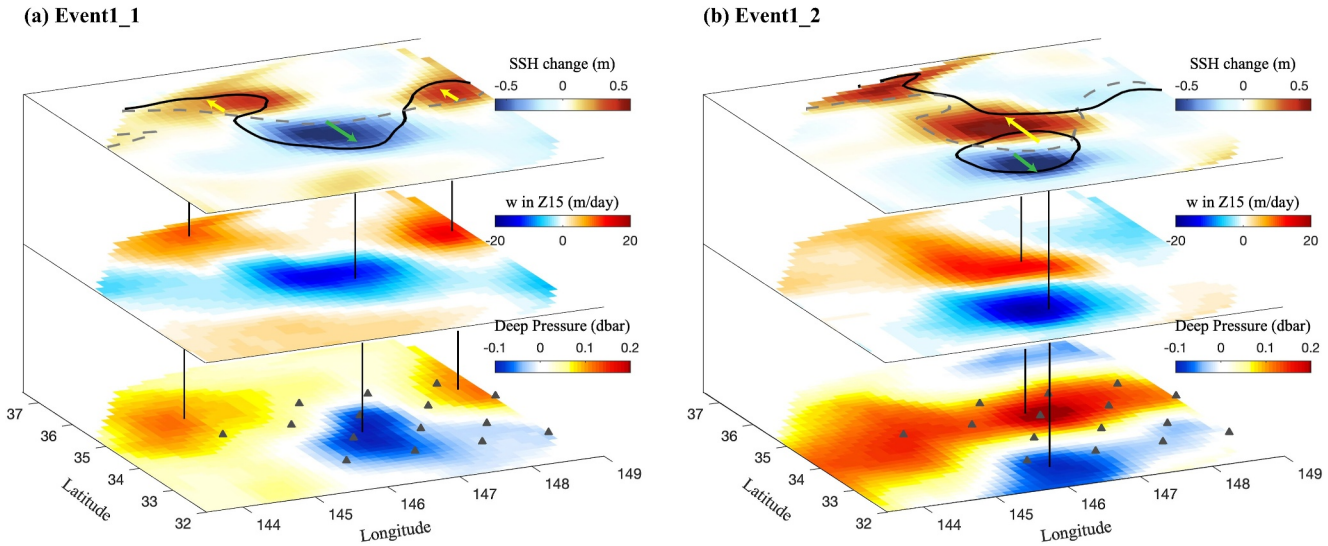

Figure 8. The first DVC event (Event1). The Event1 is divided into two stages (Event1_1 and Event1_2). (a) Coupled process in Event1_1. Upper panel: Kuroshio Extension jet movements and the SSH changes (*m*, shading). The dashed line denotes the path of Kuroshio Extension jet (2.2 m contours of SSH) at the beginning of Event1_1 (20 November 2004). The black line denotes the path of Kuroshio Extension jet at the end of Event1_1 (5 December 2004). Middle panel: mean vertical velocity of Z15 (*m/day*, shading). Lower Panel: mean deep-ocean pressure anomaly (*dbar*, shading) during event1_1. (b) As for (a), but for the Event1_2. The dashed line denotes the path of Kuroshio Extension jet at the beginning of event1_2 (6 December 2004). The black line denotes the path of Kuroshio Extension jet in the end of event1_2 (20 December 2004). The triangle markers present D4, D5, D6, E3, E4, E5, E6, E7, F4, F5, F6, G3, G4, G5 and G6 observation sites. The yellow arrow indicates KE jet is northward moving, while the blue arrow indicates KE jet southward moving.

In Event1_2 (Figure 8b), the well-developed trough pinched off to form a cold eddy and the KE jet retracted to the north. This process aligns with the one of eddy generation mechanisms: the meander of flow path leading to the eddy generation (Ji et al., 2018). The DVC process continued to play a role during this stage. The southward movement of the cold eddy led to an elevation in Z15 at its forefront. This change resulted in a net horizontal divergence within the water column, creating a low-pressure center at a depth of 5,300 m, as shown in Figures S4c–d and S8b in Supporting Information S1. Concurrently, the northward retraction of the KE jet deepened the Z15, contributing to the formation of positive pressure anomalies in the deep ocean. This positive anomaly combined with the positive pressure anomalies formed by the crests in Event1_1, culminating in a widespread

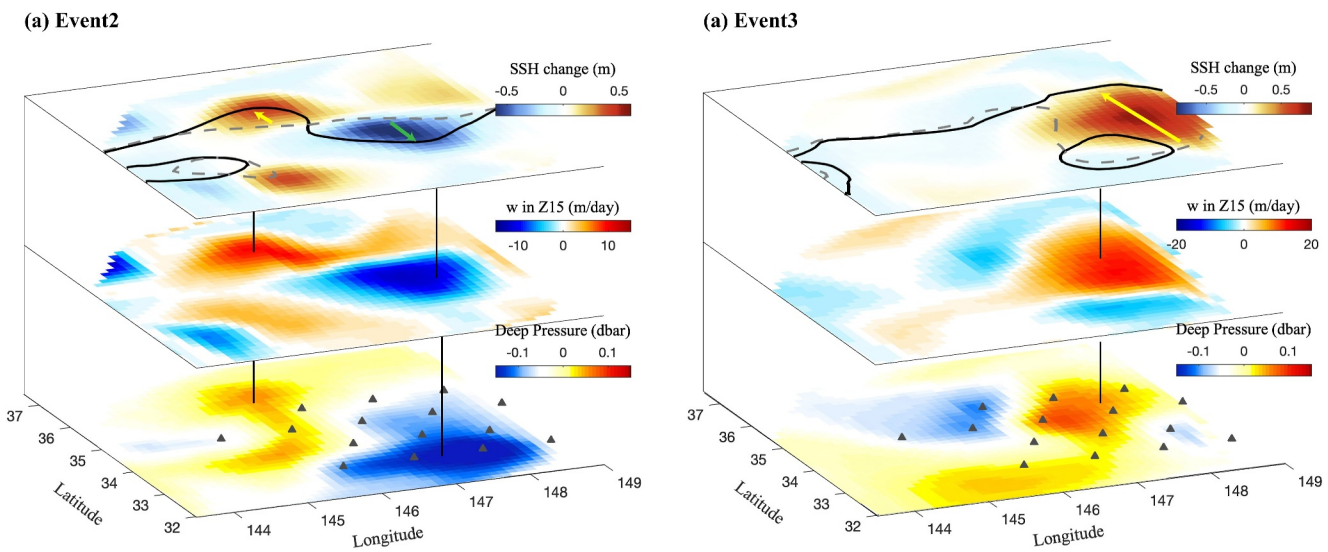

Figure 9. Same as for Figure 8, but for the Event2 and Event3. (a) The dashed line denotes the path of Kuroshio Extension jet (2.2 m contours of SSH) at the beginning of Event2 (5 March 2005). The black line denotes the path of Kuroshio Extension jet at the end of Event2 (20 March 2005). (b) The dashed line denotes the path of Kuroshio Extension jet at the beginning of Event3 (10 May 2005). The black line denotes the path of Kuroshio Extension jet at the end of Event3 (5 June 2005).

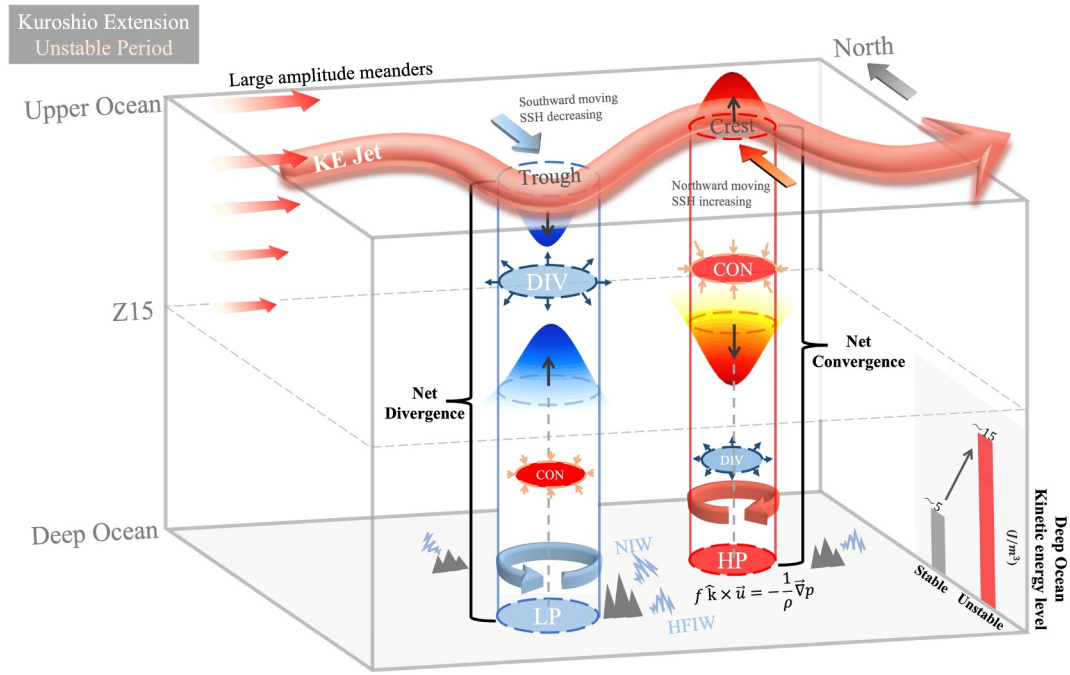

Figure 10. Schematic diagram of Dynamic Vertical Coupling process and the generation of deep eddies, NIWs and HFIWs under the influence of bottom topography. DIV represents divergence, and CON represents convergence. LP represents deep-ocean low pressure center; HP represents deep-ocean high pressure center.

area of high pressure in the deep ocean. The correlation coefficient between deep-ocean pressure and *w* throughout Event1 surpasses 0.81 at a 95% confidence level, providing statistical evidence of the DVC mechanism in this region.

Figure 9 further illustrates the DVC process for both Event2 and Event3. During Event2, a northwestward-moving cyclonic eddy merged with the southward-migrating KE jet (Figure S3 in Supporting Information S1). In this scenario, the interaction between the mesoscale eddy and the KE jet creates a strong trough downstream and an amplified crest upstream. The trough (crest) resulted in a decrease (increase) in SSH, an ascent (descent) of Z15, with divergence (convergence) in the upper layer and convergence (divergence) in the lower layer (Figure S5a–b in Supporting Information S1). This induced a net divergence (convergence) within the water column, leading to a negative (positive) pressure anomaly in the deep ocean (Figure 9, lower panel). Simultaneously, geostrophic-scale pressure anomalies at 5,300 m triggered a doubling of deep-ocean MEK to 13.52 J/m^3. As for Event3, it is similar to the DVC process of Event1_2. During this time, the path of the KE jet trough retracted northward back to 36°N (Figure 9b). This retraction resulted in an increase in SSH, a descent of Z15, with convergence in the upper layer and divergence in the lower layer. It induced a net convergence in the water column, resulting in a positive pressure anomaly in the deep ocean, which is responsible for the increase of the deep ocean MEK at 5,300 to 15.01 J/m^3 (Figure 7e). This result is consistent with the conclusion in the SVD analysis that the KE jet in the unstable mode causes an increase in deep-ocean kinetic energy.

The DVC mechanism can be illustrated in the schematic diagram as shown in Figure 10. This illustration captures the intricacies of the SSH and Z15 to the KE jet. Since the SSH (Z15) of the KE jet is tilted up (down) to the south, the southward meander (trough) of the KE jet will cause a decrease in the SSH and an increase in the Z15 in the vicinity of the jet's trough, which will inevitably cause a net divergence within the water column, as shown in Figure 10. This net divergence leads to pressure anomalies that trigger geostrophic currents in the deep ocean. The northward meander (crest), on the other hand, showed an opposite pattern. The meandering of KE jets is essentially an oceanic mesoscale instability process. The instability process represents a vertical adjustment of the center of gravity of the water mass. Essentially, this is a way to transfer the mechanical energy in the upper ocean to the deep ocean, that is, to convert the potential energy of the upper ocean into deep kinetic energy via pressure work.

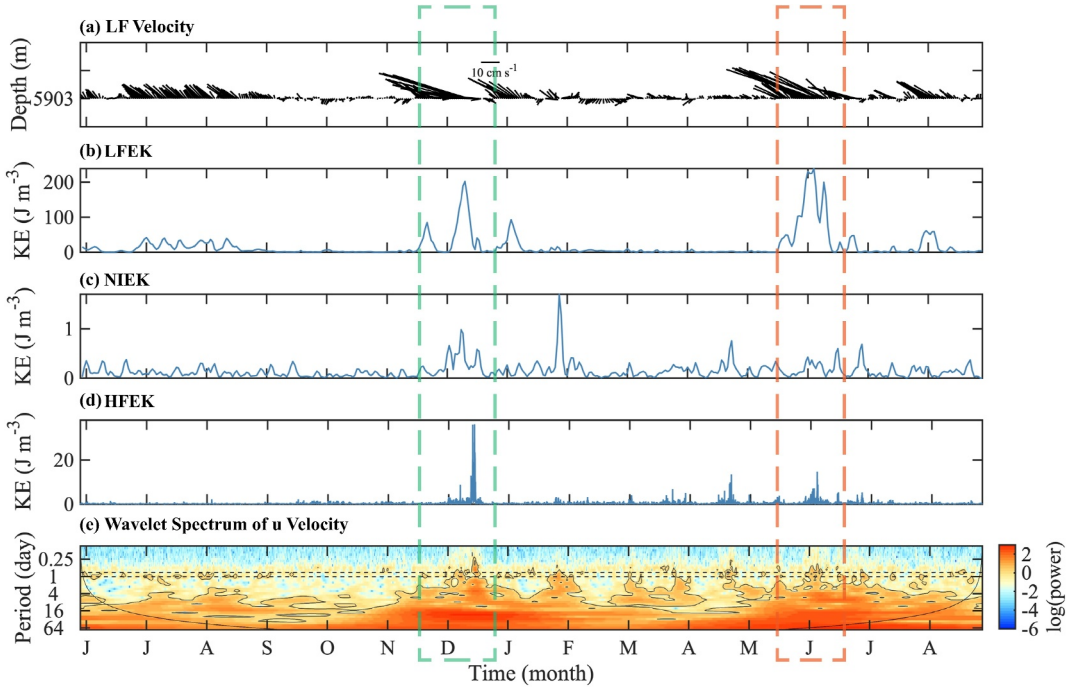

Figure 11. (a) Time series of LF velocity in E5 station. (b)–(d) Time series of LFEK, NIEK, and HFEK, respectively. (e) Wavelet power spectra of the westward velocity. The black solid contours indicate the 90% confidence level. The near-inertial band is underlined with two horizontal dashed lines.

Because the motion of mesoscale eddies can alter the depth of the thermocline, thereby inducing net convergence or divergence within the water column, they may also contribute to the variability of deep-sea kinetic energy (Xu et al., 2009). During the three events, mesoscale eddies were observed moving around the KE region (Figures S2 and S3 in Supporting Information S1). Figure S2 in Supporting Information S1 reveals a mesoscale eddy migrating westward in the south of KE jet during Event1, appearing intricately linked to the genesis of KE jet meander and subsequent cut-off eddy formation. However, as the KE jet meander developed, the mesoscale eddy underwent attenuation and was nearly stationary, with no conspicuous presence of a pronounced pressure anomaly center associated with the eddy (southeast corner of the observational array, Figure 8). This indicates that surface mesoscale eddies might not always be the dominant drivers of deep-ocean pressure anomalies. In addition, the further development of KE jet meanders during Event 1 directly contributed to the formation of the eddy (Ji et al., 2018). This suggests that KE jet meanders were a primary driver of deep ocean pressure anomalies during Event 1. The mesoscale eddies may have an impact on deep-ocean variability during Event2. A northwestward-moving cyclonic eddy merged with the southward-migrating KE jet (red box in Figure S3 in Supporting Information S1). In this scenario, the interaction between the mesoscale eddy and the KE jet contributed to the amplification of deep-ocean pressure anomalies (Figure 9a). This suggests that mesoscale eddies, when interacting with the KE jet, have a significant influence on deep-sea flow variations. As the KE jet typically extends much deeper into the water column than eddies, the rapid migration of the KE jet during unstable periods is likely to induce greater vertical movement within the thermocline than eddies. Transitioning from Event2 to Event3, the KE jet maintained a pronounced meandering pattern and quasi-stationary behavior, particularly within the trough region. During the Event3, the well-developed trough pinched off to form a cyclonic eddy and the KE jet retracted to the north quickly. The variability exhibited by the KE jet during event 3 mirrors that observed during event 1_2, both of which are indicative of the eddy generation process by flow meandering (Ji et al., 2018). Thus, KE jet meanders and mesoscale eddies together influence the variability of deep ocean currents. Nevertheless, their interaction and influences are complex and warrant further investigation.

4. Elevated Deep-Ocean Energy Cascade

The variability of the upper-ocean KE jet is mainly driven by the changes in the wind stress curl (Qiu & Chen, 2005). The DVC process could be a key mechanism for transferring WPI to the deep ocean, hence

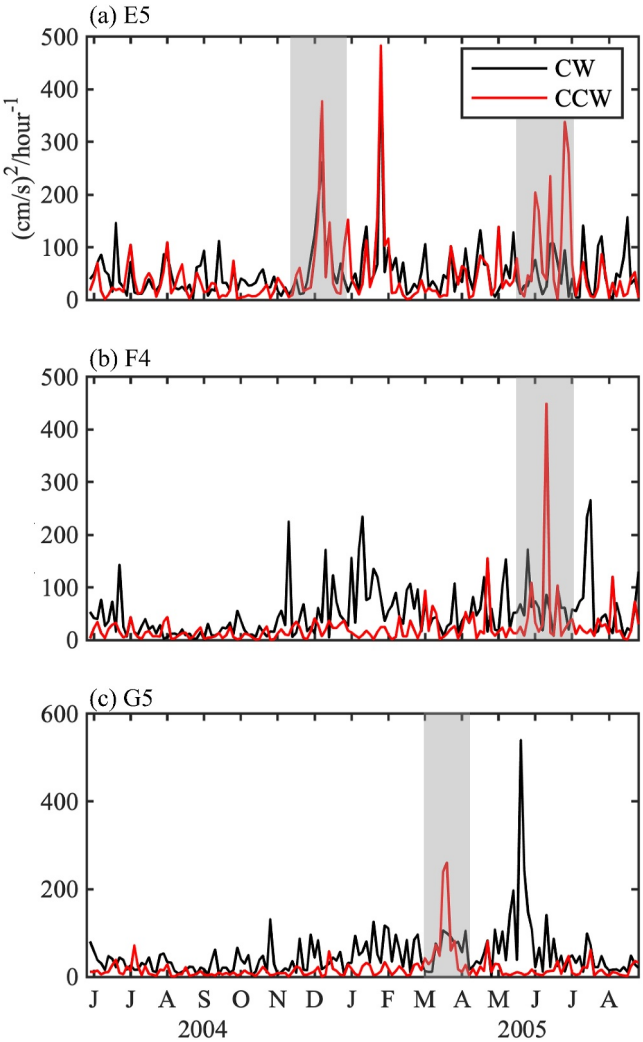

Figure 12. (a), (b) and (c) Rotary spectra of E5, F4, and G5 observed velocity, respectively. The black and red curves refer to the CW and CCW variances of NIWs computed in 3 day windows, respectively. Shaded period indicates Event1, Event2, and Event3.

intensifying the ocean interior diapycnal mixing. This mixing has a crucial role in the meridional overturning and heat budget of the ocean (Munk & Wunsch, 1998; Polzin et al., 1997; Waterhouse et al., 2014). To further examine the DVC process induced deep-ocean energy transfer and cascade from large to small scales, we analyze the energy variability at various frequency bands for the E5, G5 and F4 observation sites, which had the largest energy response in the different events (Figure 11, Figures S6 and S7 in Supporting Information S1). Consider the E5 station as an illustrative case. In Event1 and Event3, the E5 current meter at 5,903 m captured two deep flow pulses (Figure 11), with a peak LF velocity of 62 cm/s. Near the bottom level, the LFKE was two orders of magnitude larger than the background level for the two events. In addition, the energy of deep ocean near-inertial waves (NIWs) also increased considerably during DVC events (Figure 11c). The average NIEK was roughly 0.09 J/m^3 during the stable period of KE jet and jumped to an average of 0.59 J/m^3 during the events. The correlation coefficient between the LFEK and NIEK was 0.48 ~ 0.58 during events, indicating deep-ocean cascade. A wavelet analysis was applied to the time series of observed deep-ocean velocity data. Consistent with the previous findings (Hu et al., 2020; Liang & Thurnherr, 2012), during the DVC events (upper-ocean instability), the power of the velocity in the near-inertial band was enhanced by 1–2 orders at the 90% confidence level (Figure 11e). The similar process can be observed in F4 and G5 sites (Figures S6 and S7 in Supporting Information S1).

As previous research shows, NIWs over rough topography can be cascaded through various mechanisms such as large-scale flows, eddies, tides associated with the breaking of lee waves, internal tides, adjustments in the bottom Ekman layer, and the mixing of fluids (Hu et al., 2020; Liang & Wunsch, 2015; Nikurashin & Ferrari, 2010a, 2010b; Nikurashin & Legg, 2011; Xie et al., 2023). However, the mechanism of deep-ocean NIWs generation in this region is beyond the scope of this paper. What is known is that the deep-ocean topography in the KE region is characterized by rugged and complicated features, which are favorable to the generation of deep-ocean NIWs (Figure 1). The rotation spectrum analysis reveals that the counter-clockwise (CCW) phase variation exceeded the clockwise (CW) phase variation by over 50% during the DVC events (Figure 12), indicating the dominant upward energy propagation. Generally, the CCW variance was much smaller than the CW variance in the Northern Hemisphere, indicating the dominant downward energy propagation (Alford et al., 2012; Hu et al., 2020; Zhang et al., 2018). The results suggest that the generation of NIWs is attributed to the interaction between the deep ocean eddies and topography, instead being propagated from upper ocean.

In Figure 11d, the greatly enhanced deep-sea HFEK during the events suggests that the deep-sea energy induced by DVC process contributes to abyssal mixing. The HFEK near the E5 station is less than 0.7 J/m^3 when KE jet is stable, but it increased to more than 30 J/m^3 in Event1 and 10 J/m^3 in Evnet3. The wavelet analysis shows some peaks [$f, fm_2, 2f2m_2, 2f2k_1$] enhanced significantly and was identified above the 90% confidence level (Figure S8 in Supporting Information S1). This finding suggests that NIWs catalyze nonlinear wave-wave interaction (van Haren et al., 2002; Hu et al., 2020). Analogous findings may be derived by examining the energy fluctuation of F4 and G5 stations. In summary, the deep-ocean kinetic energy and diapycnal mixing can be a response to the upper-ocean KE jet variability via DVC process. The possible dynamic chain is that deep-sea eddies driven by great meanders of KE jet strike rough topography, producing NIWs and further catalyze nonlinear wave-wave interactions to excite deep-sea mixing.

5. Discussion

We provide evidence for the dynamic interaction between upper and deep ocean currents, as well as a mechanism for energy transfer from the surface to the abyssal sea. The correlation found between KEJPI and the mean kinetic energy of deep-ocean geostrophic circulation is notable, with a correlation coefficient of 0.73. This strong correlation suggests that the large amplitude meanders of the KE jet play a significant role in influencing the kinetic energy in the deep ocean, an insight that could have far-reaching implications for understanding oceanic energy dynamics. The SVD analysis has effectively unveiled a co-evolving spatial pattern between upper and lower ocean kinetic energy. By accounting for nearly 50% of the total variance, SVD1 reveals a co-evolving spatial pattern between upper and lower ocean kinetic energy. This analytical approach provides a more nuanced understanding of coupled variation in the upper-ocean KE jet and the kinetic energy of deep-ocean geostrophic flows.

We delve further into the DVC mechanism. The substantial coherence between SSH, Z15, deep pressure anomaly, and abyssal flow suggests that KE jet migration can cause net divergence or convergence within the water column, resulting in deep pressure anomalies. These pressure anomalies can subsequently form deep-ocean quasi-geostrophic currents, which have been found to bring about a considerable increase in kinetic energy in the deep ocean, sometimes reaching levels three times greater than the background. It is consistent with the conclusion in the SVD analysis that the KE jet in the unstable mode causes an increase in deep-ocean kinetic energy in most areas. DVC analysis elucidates the dynamic processes underlying specific events that contribute to the statistical correlation between the co-evolving kinetic energy of the upper and deep ocean. The results of the SVD analyses provide statistical evidence of the relationship between *GEK_u* and *GEK_d*, which does not necessarily guarantee the same spatial pattern between SVD1 *GEK_u* and *GEK_d* from an ocean dynamics perspective. It is the migration rather than the kinetic energy level of the KE jet that induces variability in the deep ocean. The *GEK_d* variability (Figure 5b) should be related to the upper ocean KE jet path variability (Figure 4b).

We also show that DVC-driven kinetic energy can cascade into near-inertial and high-frequency internal waves, contributing to abyssal mixing. The whole process is illustrated in Figure 10. It underscores the role of large current system instabilities, such as those in the KE jet meandering, in transferring energy to the deep ocean and highlights their importance in facilitating deep mixing processes that are critical for understanding global ocean circulation and climate.

Data Availability Statement

The deep ocean velocity, deep pressure variations and the vertical acoustic travel time during observations were from http://www.po.gso.uri.edu/dynamics/KESS/CPIES_data.html. Further documentation about data processing is available at https://digitalcommons.uri.edu/physical_oceanography_techrpts/1/. Bathymetry data of the Kuroshio Extension are from SRTM15_PLUS (https://topex.ucsd.edu/www_html/mar_%20topo.html). The climatological SSH data is from https://data.marine.copernicus.eu/product/SEALEVEL_GLO_PHY_MDT_008_063/download?dataset=cnes_obs-sl_glo_phy-mdt_my_0.125deg_P20Y_202012–ext–mdt. The daily SSH data is from https://data.marine.copernicus.eu/product/SEALEVEL_GLO_PHY_CLIMATE_L4_MY_008_057/.

Acknowledgments
Thanks to the two anonymous reviewers for their suggestions and help us revise the manuscript. Thanks for the helpful discussions and suggestions from Qirong An, Yuhui Zhao and Jianping Gan. We are grateful to the KESS program for providing high-quality data, and to the KESS project team for their early efforts and research results. This work was supported in part by Laoshan Laboratory science and technology innovation projects (LSKJ202201406-2), NSFC-Shandong Joint Fund Key Project (U22A20587), Innovative Practice Training Program of University of the National Academy of Sciences (Y5KY09101 L), in part by the National Key Research and Development Program Grant 2019YFC1509102, in part by the National Natural Science Foundation of China under Grant 41676168 and Grant 41906027, and in part by the NSFC-Shandong Joint Fund for Marine Science Research Centers under Grant U1406401.

References

Adams, D. K., & Flierl, G. R. (2010). Modeled interactions of mesoscale eddies with the East Pacific Rise: Implications for larval dispersal. *Deep Sea Research Part I: Oceanographic Research Papers*, *57*(10), 1163–1176. https://doi.org/10.1016/j.dsr.2010.06.009

Alford, M. H., Cronin, M. F., & Klymak, J. M. (2012). Annual cycle and depth penetration of wind-generated near-inertial internal waves at ocean station papa in the northeast pacific. *Journal of Physical Oceanography*, *42*(6), 889–909. https://doi.org/10.1175/JPO-D-11-092.1

Andres, M., Wimbush, M., Park, J.-H., Chang, K.-I., Lim, B.-H., Watts, D. R., et al. (2008). Observations of Kuroshio flow variations in the east China sea. *Journal of Geophysical Research*, *113*(C5), C05013. https://doi.org/10.1029/2007JC004200

Bishop, S. P. (2013). Divergent eddy heat fluxes in the Kuroshio extension at 144°–148°E. Part II: Spatiotemporal variability. *Journal of Physical Oceanography*, *43*(11), 2416–2431. https://doi.org/10.1175/JPO-D-13-061.1

Cai, Z., & Gan, J. (2021). Dynamics of the layered circulation inferred from kinetic energy pathway in the south China sea. *Journal of Physical Oceanography*, *51*(5), 1671–1685. https://doi.org/10.1175/JPO-D-20-0226.1

Donohue, K. A., Watts, D. R., Tracey, K. L., Greene, A. D., & Kennelly, M. (2010). Mapping circulation in the Kuroshio extension with an array of current and pressure recording inverted echo sounders. *Journal of Atmospheric and Oceanic Technology*, *27*(3), 507–527. https://doi.org/10.1175/2009JTECHO686.1

Greene, A. D., Watts, D. R., Sutyrin, G. G., & Sasaki, H. (2012). Evidence of vertical coupling between the Kuroshio extension and topographically controlled deep eddies. *Journal of Marine Research*, *70*(5), 719–747. https://doi.org/10.1357/002224012806290723

Hu, Q., Huang, X., Zhang, Z., Zhang, X., Xu, X., Sun, H., et al. (2020). Cascade of internal wave energy catalyzed by eddy-topography interactions in the deep south China sea. *Geophysical Research Letters*, *47*(4), e2019GL086510. https://doi.org/10.1029/2019GL086510

Ji, J., Dong, C., Zhang, B., Liu, Y., Zou, B., King, G. P., et al. (2018). Oceanic eddy characteristics and generation mechanisms in the Kuroshio Extension region. *Journal of Geophysical Research: Oceans*, *123*(11), 8548–8567. https://doi.org/10.1029/2018JC014196

Kennelly, M., Donohue, K., Greene, A., Tracey, K. L., & Watts, D. R. (2008). *Inverted echo sounder data report, Kuroshio extension system study (KESS) april 2004 to july 2006. GSO technical report 2008-02*. University of Rhode Island.

Kohyama, T., Yamagami, Y., Miura, H., Kido, S., Tatebe, H., & Watanabe, M. (2021). The Gulf Stream and Kuroshio current are synchronized. *Science*, *374*(6565), 341–346. https://doi.org/10.1126/science.abh3295

Liang, X., & Thurnherr, A. M. (2011). Subinertial variability in the deep ocean near the East Pacific Rise between 9° and 10°N. *Geophysical Research Letters*, *38*(6), L06606. https://doi.org/10.1029/2011GL046675

Liang, X., & Thurnherr, A. M. (2012). Eddy-modulated internal waves and mixing on a midocean ridge. *Journal of Physical Oceanography*, *42*(7), 1242–1248. https://doi.org/10.1175/JPO-D-11-0126.1

Liang, X., & Wunsch, C. (2015). Note on the redistribution and dissipation of tidal energy over mid-ocean ridges. *Tellus A: Dynamic Meteorology and Oceanography*, *67*(1), 27385. https://doi.org/10.3402/tellusa.v67.27385

Meinen, C. S., & Watts, D. R. (2000). Vertical structure and transport on a transect across the North Atlantic Current near 42°N: Time series and mean. *Journal of Geophysical Research*, *105*(C9), 21869–21891. https://doi.org/10.1029/2000JC900097

Munk, W., & Wunsch, C. (1998). Abyssal recipes II: Energetics of tidal and wind mixing. *Deep-Sea Research*, *45*(12), 1977–2010. https://doi.org/10.1016/S0967-0637(98)00070-3

Na, H., Watts, D. R., Park, J.-H., Jeon, C., Lee, H. J., Nonaka, M., & Greene, A. D. (2016). Bottom pressure variability in the Kuroshio Extension driven by the atmosphere and ocean instabilities. *Journal of Geophysical Research: Oceans*, *121*(8), 6507–6519. https://doi.org/10.1002/2016JC012097

Nikurashin, M., & Ferrari, R. (2010a). Radiation and dissipation of internal waves generated by geostrophic motions impinging on small-scale topography: Theory. *Journal of Physical Oceanography*, *40*(5), 1055–1074. https://doi.org/10.1175/2009JPO4199.1

Nikurashin, M., & Legg, S. (2011). A mechanism for local dissipation of internal tides generated at rough topography. *Journal of Physical Oceanography*, *41*(2), 378–395. https://doi.org/10.1175/2010JPO4522.1

Petersen, M. R., Williams, S. J., Maltrud, M. E., Hecht, M. W., & Hamann, B. (2013). A three-dimensional eddy census of a high-resolution global ocean simulation: 3-D global eddy census. *Journal of Geophysical Research*, *118*(4), 1759–1774. https://doi.org/10.1002/jgrc.20155

Polzin, K. L., Toole, J. M., Ledwell, J. R., & Schmitt, R. W. (1997). Spatial variability of turbulent mixing in the abyssal ocean. *Science*, *276*(5309), 93–96. https://doi.org/10.1126/science.276.5309.93

Qiu, B., & Chen, S. (2005). Variability of the Kuroshio extension jet, recirculation gyre, and mesoscale eddies on decadal time scales. *Journal of Physical Oceanography*, *35*(11), 2090–2103. https://doi.org/10.1175/JPO2807.1

Savidge, D. K., & Bane, J. M. (1999). Cyclogenesis in the deep ocean beneath the Gulf Stream: 2. Dynamics. *Journal of Geophysical Research*, *104*(C8), 18127–18140. https://doi.org/10.1029/1999JC900131

Scott, R. B., & Xu, Y. (2009). An update on the wind power input to the surface geostrophic flow of the World Ocean. *Deep Sea Research Part I: Oceanographic Research Papers*, *56*(3), 295–304. https://doi.org/10.1016/j.dsr.2008.09.010

Shay, T. J., Bane, J. M., Watts, D. R., & Tracey, K. L. (1995). Gulf Stream flow field and events near 68°W. *Journal of Geophysical Research*, *100*(C11), 22565–22589. https://doi.org/10.1029/95JC02685

Tracey, K. L., Watts, D. R., Donohue, K. A., & Ichikawa, H. (2012). Propagation of Kuroshio extension meanders between 143° and 149°E. *Journal of Physical Oceanography*, *42*(4), 581–601. https://doi.org/10.1175/JPO-D-11-0138.1

van Haren, H., Maas, L., & van Aken, H. (2002). On the nature of internal wave spectra near a continental slope. *Geophysical Research Letters*, *29*(12). https://doi.org/10.1029/2001GL014341

Venegas, S. A., Mysak, L. A., & Straub, D. N. (1997). Atmosphere–Ocean coupled variability in the south atlantic. *Journal of Climate*, *10*(11), 2904–2920. https://doi.org/10.1175/1520-0442(1997)010<2904:AOCVIT>2.0.CO;2

Wallace, J. M., Smith, C., & Bretherton, C. S. (1992). Singular value decomposition of wintertime sea surface temperature and 500-mb height anomalies. *Journal of Climate*, *5*(6), 561–576. https://doi.org/10.1175/1520-0442(1992)005<0561:SVDOWS>2.0.CO;2

Waterhouse, A. F., MacKinnon, J. A., Nash, J. D., Alford, M. H., Kunze, E., Simmons, H. L., et al. (2014). Global patterns of diapycnal mixing from measurements of the turbulent dissipation rate. *Journal of Physical Oceanography*, *44*(7), 1854–1872. https://doi.org/10.1175/JPO-D-13-0104.1

Watts, D. R., & Johns, W. E. (1982). Gulf Stream meanders: Observations on propagation and growth. *Journal of Geophysical Research*, *87*(C12), 9467–9476. https://doi.org/10.1029/JC087iC12p09467

Watts, D. R., & Rossby, H. T. (1977). Measuring dynamic heights with inverted echo sounders: Results from MODE. *Journal of Physical Oceanography*, *7*(3), 345–358. https://doi.org/10.1175/1520-0485(1977)007<0345:MDHWIE>2.0.CO;2

Watts, D. R., Sun, C., & Rintoul, S. (2001). A two-dimensional gravest empirical mode determined from hydrographic observations in the subantarctic front. *Journal of Physical Oceanography*, *31*(8), 2186–2209. https://doi.org/10.1175/1520-0485(2001)031<2186:ATDGEM>2.0.CO;2

Watts, D. R., Tracey, K. L., Bane, J. M., & Shay, T. J. (1995). Gulf Stream path and thermocline structure near 74°W and 68°W. *Journal of Geophysical Research*, *100*(C9), 18291–18312. https://doi.org/10.1029/95JC01850

Xie, X., Wang, Y., Liu, Z., Liu, X., Chen, D., Zhang, D., & Wang, J. (2023). Observation of near-inertial waves in the bottom boundary layer of an abyssal seamount. *Journal of Physical Oceanography*, *53*(2), 635–645. https://doi.org/10.1175/JPO-D-22-0026.1

Xu, Y., & Scott, R. B. (2008). Subtleties in forcing eddy resolving ocean models with satellite wind data. *Ocean Modelling*, *20*(3), 240–251. https://doi.org/10.1016/j.ocemod.2007.09.003

Xu, Y., Watts, D. R., & Wimbush, M. (2009). Coupled patterns between fields of dynamic height and bottom pressure in the Japan/East Sea. *Ocean Science Journal*, *44*(1), 35–42. https://doi.org/10.1007/s12601-009-0005-4

Yang, Y., Liang, X. S., & Sasaki, H. (2021). Vertical coupling and dynamical source for the intraseasonal variability in the deep Kuroshio Extension. *Ocean Dynamics*, *71*(11–12), 1069–1086. https://doi.org/10.1007/s10236-021-01482-9

Zhang, Y., Liu, Z., Zhao, Y., Li, J., & Liang, X. (2015). Effect of surface mesoscale eddies on deep-sea currents and mixing in the northeastern South China Sea. *Deep Sea Research Part II: Topical Studies in Oceanography*, *122*, 6–14. https://doi.org/10.1016/j.dsr2.2015.07.007

Zhang, Z., Qiu, B., Tian, J., Zhao, W., & Huang, X. (2018). Latitude-dependent finescale turbulent shear generations in the Pacific tropical-extratropical upper ocean. *Nature Communications*, *9*(1), 4086. https://doi.org/10.1038/s41467-018-06260-8

Zhang, Z., Zhao, W., Tian, J., & Liang, X. (2013). A mesoscale eddy pair southwest of Taiwan and its influence on deep circulation: Mesoscale eddy southwest of taiwan. *Journal of Geophysical Research*, *118*(12), 6479–6494. https://doi.org/10.1002/2013JC008994